Jurnal Presipitasi
Media Komunikasi dan Pengembangan Teknik Lingkungan
e-ISSN: 2550-0023

Vol 23, No 3, 2026,
Article available at homepage presipitasi

Original Research Article

Land-Cover Trajectories and Potential Runoff Sensitivity in the Welang Watershed

Rizki Tri Utami[1*], Ussy Andawayanti[2], Ery Suhartanto[2], Rahmah Dara Lufira[2], Rizki Ramadhani Pratama[3]

[1] Magister Program, Department of Water Resources Engineering, Faculty of Engineering, Universitas Brawijaya, Jalan MT Haryono 167, Malang, Indonesia 65145

[2]Department of Water Resources Engineering, Faculty of Engineering, Universitas Brawijaya, Jalan MT Haryono 167, Malang, Indonesia 65145

[3]Department of Civil and Environmental Engineering, Nagoya University, Furo-cho, Chikusa-ku, Nagoya, Aichi, Japan 464-8603

* Corresponding Author, email: rizkiutami1653@gmail.com

Copyright ©2026 by Authors,
Published by Environmental Engineering Department,
Faculty of Engineering, UniversitasDiponegoro
This open accessarticle is distributed under a
Creative Commons Attribution 4.0 International License

Abstract

Land-cover conversion modifies watershed surface characteristics, but satellite-derived maps alone cannot quantify changes in discharge or flood magnitude. This study evaluated land-cover trajectories in the 522.90 km² Welang watershed, East Java, Indonesia, over a 19-year elapsed period (2004–2023). Landsat 7 Enhanced Thematic Mapper Plus imagery was used for 2004 and 2009, and Landsat 8 Operational Land Imager imagery for 2014, 2019, and 2023. Supervised Maximum Likelihood Classification distinguished water bodies, open land, built-up area, agricultural land, and vegetation. Classification reliability was evaluated using producer's accuracy, user's accuracy, overall accuracy, and the Kappa coefficient. Built-up area increased by 34.87 km², agricultural land by 27.94 km², and vegetation decreased by 45.52 km². The combined proportion of built-up and agricultural land increased from 50.96% to 62.97%. Producer's and user's accuracies were generally high, and overall accuracy ranged from 90.00% to 93.33%. Beyond documenting land-cover change, these trajectories indicate a shift toward surface conditions with greater potential sensitivity to rapid runoff generation and erosion. Because rainfall–runoff response was not calibrated against the mapped land-cover states, the results indicate potential hydrological sensitivity rather than measured flood amplification. The results support vegetation protection, agricultural soil conservation, stormwater-sensitive planning, and calibrated hydrological modeling.

Keywords: Agriculture; classification; landsat; runoff; urbanization; vegetation

1. Introduction

Land-cover change is an important anthropogenic control on watershed surface conditions and hydrological processes. Converting vegetated land to cultivated, exposed, or developed surfaces can alter rainfall interception, evapotranspiration, infiltration opportunities, soil protection, surface roughness, and the connectivity of overland flow pathways. These mechanisms are particularly important in humid tropical watersheds, where high-intensity rainfall interacts with steep terrain, erodible soils, expanding settlements, and intensive agricultural activity. Calibrated watershed studies have demonstrated that

land-cover conversion can modify surface runoff, streamflow components, sediment production, and flood response, although the direction and magnitude of the response depend on rainfall characteristics, soil properties, topography, drainage connectivity, and the spatial position of converted areas within a watershed (Banjara et al., 2024; Costa et al., 2023; Sadhwani et al., 2022). Accordingly, land-cover trajectories are hydrologically meaningful not merely as indicators of landscape change, but as evidence of shifts in surface characteristics that regulate runoff generation, erosion susceptibility, and the transfer of water and sediment through a watershed.

Long-term Earth-observation archives provide an effective means of reconstructing landscape transformation where consistent field observations are limited. Landsat imagery is particularly suitable for watershed-scale assessments because its 30 m spatial resolution and multi-decadal continuity enable comparable observations over extended periods. Multi-temporal Landsat analyses have increasingly been integrated with cloud computing platforms, machine learning algorithms, terrain information, phenological variables, and independent validation datasets to improve the consistency and reliability of land-cover mapping (Al-Taei et al., 2023; Amini et al., 2022; Dash et al., 2023).

The selected classification algorithm alone does not determine the reliability of land-cover classification. Acquisition season, crop phenology, atmospheric conditions, antecedent surface moisture, spectral-band selection, terrain effects, training-sample design, and the independence of validation samples can substantially affect the resulting maps. These factors are particularly important in heterogeneous agricultural landscapes because harvested fields, exposed soil, sparse vegetation, and some built materials can exhibit overlapping spectral responses (Ibrahim, 2023; Melichar et al., 2023). Classification uncertainty must therefore be evaluated explicitly before using land-cover maps for environmental or hydrological interpretation. Hydrological interpretation requires evidence beyond remote-sensing classification because mapped land-cover change alone does not establish changes in runoff, discharge, flood magnitude, or sediment response. Precipitation variability, soil properties, topography, drainage density, and flow-path connectivity can modify the hydrological expression of similar land-cover changes (Alexopoulos et al., 2023; Chawanda et al., 2024; Gebrechorkos et al., 2024; Liu et al., 2025).

Land-cover transformation also influences erosion, sediment transport, seasonal water availability, and the economic value of watershed resources. Vegetation loss and agricultural expansion on erosion-prone terrain may increase soil detachment and sediment delivery, particularly where conservation practices are inadequate. Watershed-conservation planning should therefore consider both the magnitude of land-cover change and the spatial relationship among land cover, erosion susceptibility, and sediment transport (Lufira et al., 2022). Agricultural erosion can also be reduced through locally appropriate structural and vegetative measures, including environmentally compatible sediment-retention systems (Haribowo et al., 2019). At a broader management level, spatial information on land-use allocation can support optimization of water allocation and economic benefits when integrated with hydrological and socioeconomic considerations (Satyagraha et al., 2018).

The Welang watershed in East Java, Indonesia, provides a relevant tropical case study because it extends from the mountainous headwaters to the Pasuruan lowlands. The watershed contains a connected network of tributaries, seven rainfall stations, and a downstream Automatic Water Level Recorder. Its upstream–downstream configuration creates spatial contrasts in terrain, settlement development, agricultural activity, vegetation cover, and potential runoff connectivity. Five land-cover observations spanning 2004 to 2023 were available for analysis. However, the available hydrometeorological records were not analyzed as complete, quality-controlled rainfall and discharge series corresponding to each mapped land-cover state. Accordingly, the present study was designed not as a land-cover inventory alone, but as an integrated assessment of long-term landscape trajectories, their classification reliability, and their potential implications for runoff-generating surface conditions and watershed management. This contribution goes beyond producing five temporally separated land-cover maps by reconstructing the direction, magnitude, and persistence of watershed-scale land-cover

reorganization and evaluating whether the concurrent trajectories of vegetation, agricultural land, and built-up surfaces indicate a coherent shift in runoff-generating surface conditions. This trajectory-based perspective distinguishes persistent landscape transformation from isolated differences between individual observation years and provides a quantitative baseline for subsequent hydrological assessment and spatial watershed management.

The study therefore provides an uncertainty-aware reconstruction of long-term land-cover trajectories and their potential implications for runoff-generating conditions. Recent research in an Indonesian urban watershed demonstrated that multitemporal Landsat classification combined with a cellular automata–artificial neural network framework can identify spatial transition potential and support spatially explicit watershed-resilience planning (Lufira et al., 2026). Unlike this predictive framework, the present study reconstructs five observed land-cover states in the Welang watershed and explicitly distinguishes mapped landscape change from uncalibrated hydrological inference.

The scientific novelty of this study does not lie in using multi-temporal Landsat classification alone, nor solely in separating observed landscape change from uncalibrated hydrological inference. Rather, it lies in the trajectory-based synthesis of five observed land-cover states to determine whether changes in the major land-cover classes represent a persistent and coordinated reorganization of watershed surface conditions. By jointly evaluating the direction and temporal consistency of vegetation loss and the expansion of agricultural and built-up land, the study provides new empirical evidence of how the surface composition of the Welang watershed has progressively shifted toward conditions potentially more conducive to rapid runoff generation and erosion sensitivity. The first level comprises directly observed land-cover areas and trajectories derived from satellite-image classification. The second level comprises process-based interpretations of how the observed transformations may affect interception, infiltration opportunity, soil protection, erosion susceptibility, and runoff connectivity. The third level comprises hydrological responses that require independent hydrometeorological observations or calibrated modeling for quantitative evaluation. This distinction prevents land-cover changes from being incorrectly presented as measured hydrological responses. More importantly, it allows the mapped trajectories to be evaluated as changes in runoff-generating surface conditions rather than as purely descriptive changes in land-cover composition. Thus, the three-level evidentiary framework constrains interpretation. At the same time, the principal scientific contribution is the quantitative reconstruction and hydrologically relevant synthesis of the long-term land-cover trajectory.

The working hypothesis was that the simultaneous loss of vegetation and the expansion of built-up and agricultural land shifted the Welang watershed toward surface conditions with greater potential for rapid runoff generation. Accordingly, the objectives were to: (i) classify land cover in 2004, 2009, 2014, 2019, and 2023; (ii) evaluate the reliability of the resulting land-cover maps; (iii) quantify net, relative, percentage-point, and mean annualized changes in five land-cover classes; and (iv) interpret the potential hydrological and watershed-management significance of the observed trajectories without attributing unmeasured changes in discharge or flood magnitude.

2. Materials and Methods

2.1 Study Area and Hydrometeorological Setting

The Welang watershed is in East Java, Indonesia, and covers 522.90 km². The watershed extends from approximately 7°34′–7°57′ S and 112°35′–112°56′ E, spanning parts of Pasuruan Regency, Pasuruan City, and Malang Regency. Its physiography features volcanic highlands in the upstream region that transition to low-lying alluvial plains downstream (Suhartanto et al., 2025). Previous research in the Welang watershed reported upstream elevations of approximately 3212.5 m above sea level, while downstream areas range from approximately 0–9.25 m above sea level (Wahyudi et al., 2018). A hydrological study using the Dhompo-controlled Welang watershed delineation reported mean slopes of approximately 19.17% in the upstream area, 14.54% in the middle watershed, and 3.85% downstream, confirming the pronounced reduction in terrain gradient toward the watershed outlet (Sulianto, 2024). Its elongated

configuration and convergent drainage network connect the western and southern headwaters with the lower watershed. Seven rainfall stations monitor the watershed: Telebuk, Sengon Pager, Purwosari/Tejosari, Selowongko, Lawang, Tutur, and Wonorejo. A downstream Automatic Water Level Recorder is located near Dhompo. Figure 1 shows the watershed boundary, river network, rainfall stations, and downstream recorder. The monitoring network establishes the study area's hydrometeorological context. The rainfall stations and downstream water-level recorder were used only to establish the study area's hydrometeorological context and were not analyzed as evidence of land-cover-attributable hydrological change.

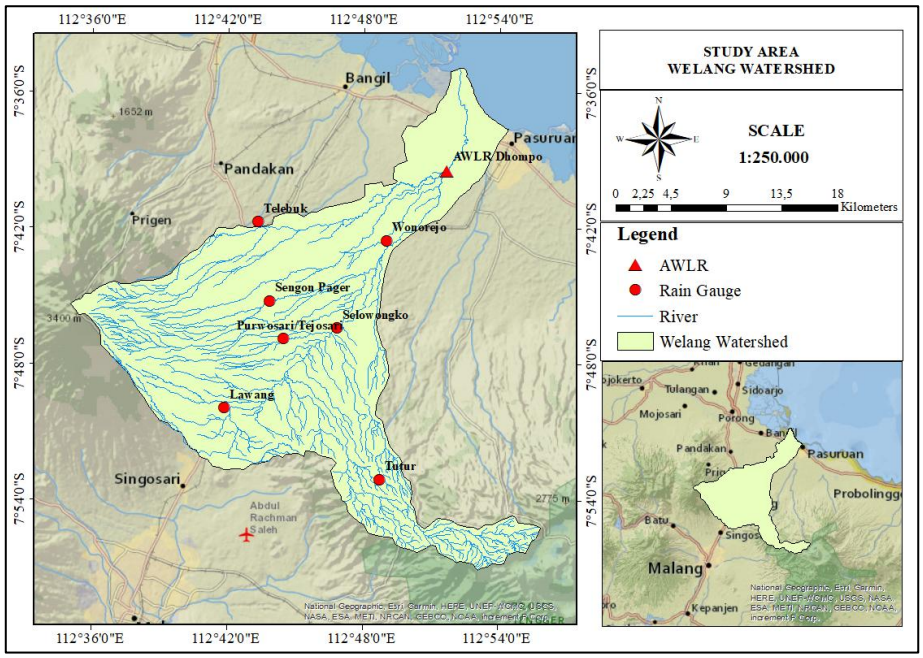


Figure 1. Study area of the Welang watershed, East Java, Indonesia

The pronounced upstream–downstream terrain gradient is hydrologically relevant because land conversion on steep, well-connected slopes may produce a different response than conversion on flatter or weakly connected surfaces. Topography and land cover can interact nonlinearly in controlling infiltration, surface runoff, subsurface flow, erosion, and sediment delivery, even between adjacent watersheds exposed to broadly similar climatic conditions (Liu et al., 2025; Lufira et al., 2022). The present study did not stratify land-cover change by slope, soil type, sub-watershed, erosion class, or distance to the stream network. These variables were therefore treated as priorities for subsequent spatial analysis rather than explanatory variables quantified in the current study.

2.2 Data Sources and Analytical Scope

The analysis used Landsat imagery, a fixed watershed boundary, river-network data, monitoring-station locations, and reference samples. Landsat 7 Enhanced Thematic Mapper Plus imagery was used for 2004 and 2009, whereas Landsat 8 Operational Land Imager imagery was used for 2014, 2019, and 2023. All images were analyzed at 30 m spatial resolution and clipped to the fixed 522.90 km² watershed boundary. The five observation years represent discrete temporal snapshots over a 19-year elapsed period from 2004 to 2023, with 5-year intervals between 2004–2009, 2009–2014, and 2014–2019, and a 4-year interval between 2019 and 2023. The analysis therefore characterizes long-term trajectories rather than continuous annual land-cover dynamics and cannot resolve annual variability, temporary clearing, crop rotation, or short-term seasonal surface exposure.

Multi-temporal Landsat data are widely used for long-term watershed-scale land-cover assessment because of their spatial consistency and extended observation record (Al-Taei et al., 2023;

Amini et al., 2022; Dash et al., 2023). The watershed boundary was used for image clipping and class-area calculation, while the river network supported spatial interpretation. Rainfall-station and downstream water-level-recorder locations were included only as hydrometeorological context because the corresponding time series were not analyzed quantitatively. Reference samples were used to calculate producer's accuracy, user's accuracy, overall accuracy, and the Kappa coefficient. Reference labels for the accuracy assessment were obtained through visual interpretation of Google Earth imagery corresponding to the same observation years as the Landsat classifications, with validation locations examined individually against the reference imagery. The validation samples were kept separate from the training samples used to develop the Maximum Likelihood classifier, thereby providing an independent basis for evaluating classification performance. The supplied analytical archive did not include complete confusion-matrix counts, reference-sample coordinates, sampling-design documentation, or class-area confidence intervals. The reported accuracy measures were therefore used to evaluate general map reliability rather than to derive design-based or area-adjusted area estimates.

2.3 Landsat Image Preprocessing

Image preprocessing was undertaken in Google Earth Engine, while ArcGIS was used for spatial inspection, watershed clipping, map preparation, and class-area calculation. Google Earth Engine provides cloud-based access to extensive Earth-observation archives and computational resources suitable for multi-temporal geospatial analysis (Gorelick et al., 2017). Relatively low-cloud images were selected, cloud- and shadow-affected pixels were excluded, and all images were clipped to the fixed Welang watershed boundary. A common 30 m spatial resolution and a consistent classification scheme were applied across all observation years to minimize differences arising from spatial extent or changes in class definitions. The principal sensor transition occurred between 2009 and 2014 because Landsat 7 ETM+ imagery was used for 2004 and 2009, whereas Landsat 8 OLI imagery was used for 2014, 2019, and 2023. Differences in spectral-response functions and radiometric characteristics between Landsat 7 ETM+ and Landsat 8 OLI may introduce discontinuities into multi-sensor time-series analyses when cross-sensor effects are not adequately considered (Roy et al., 2016). Changes during the 2009–2014 interval were therefore interpreted conservatively and evaluated together with the longer-term direction of change across all observation years.

Using Landsat 8 OLI imagery for 2014, 2019, and 2023 reduced cross-sensor inconsistency within the final three observations. Nevertheless, differences in acquisition season, crop phenology, antecedent rainfall, soil moisture, atmospheric conditions, and surface exposure could still affect discrimination among agricultural land, open land, vegetation, and built-up surfaces (Ibrahim, 2023; Melichar et al., 2023). Because Landsat 7 imagery acquired after May 2003 is affected by the Scan Line Corrector failure, localized scan-line gaps may also affect classification if not adequately addressed. Consequently, the interpretation emphasized substantial and directionally persistent watershed-scale changes rather than isolated local differences between consecutive maps.

2.4 Land-Cover Classification and Change Analysis

Supervised Maximum Likelihood Classification was applied separately to the five observation years. Five classes were mapped consistently: water bodies, open land, built-up area, agricultural land, and vegetation. A consistent classification system is essential because changes in class definition between observation years may be incorrectly interpreted as physical land-cover transitions (Al-Taei et al., 2023; Dash et al., 2023). Water bodies comprised rivers, ponds, reservoirs, and other open-water surfaces. Because Landsat imagery has a spatial resolution of 30 m, narrow river reaches may occupy only a fraction of a pixel and may therefore be represented as mixed water–land pixels. Consequently, the mapped water-body class should be interpreted as detectable open-water coverage at Landsat scale rather than as a complete representation of the geometric extent of all river channels. Open land represented exposed soil, sparsely covered ground, and recently cleared surfaces. Built-up area represented settlements,

buildings, roads, and other developed surfaces detectable at 30 m resolution. Agricultural land represented cultivated and managed fields, while vegetation comprised forest, shrub, and other densely vegetated surfaces. The classification system did not distinguish agricultural subtypes, crop calendars, forest structure, settlement density, road surfaces, or directly connected impervious area. Hydrological interpretation was therefore restricted to broad surface-condition classes rather than detailed hydrological response units. Because the five mapped classes were derived from remotely sensed surface characteristics rather than direct information on socioeconomic land functions, this study uses the term "land cover" consistently to describe the mapped classes, their spatial distributions, and their temporal changes. Terminology used in the titles or methodological descriptions of cited studies is retained where necessary to preserve the original meaning of those sources. The area of each land-cover class was calculated using Equation (1):

$$A_i = \frac{n_i \times r^2}{10^6} \quad (1)$$

where A_i is the area of land-cover class i in square kilometers, n_i is the number of pixels classified as class i, and r is the Landsat spatial resolution in meters. The factor 10^6 converts square meters to square kilometers. The percentage of each class was calculated using Equation (2):

$$P_i = \frac{A_i}{A_t} \times 100 \quad (2)$$

where P_i is the percentage of land-cover class i, A_i is the area of class i, and A_t is the total watershed area of 522.90 km². Net area change was calculated using Equation (3):

$$\Delta A_i = A_{i,2023} - A_{i,2004} \quad (3)$$

Relative change was calculated as the net area change divided by the corresponding 2004 class area and expressed as a percentage. Percentage-point change was calculated as the difference between the proportional land-cover shares in 2023 and 2004 (Pi,2023-Pi,2004). Positive values indicate expansion, whereas negative values indicate contraction of the corresponding land-cover class.

The mean annualized change over the 19-year elapsed period between 2004 and 2023 was calculated using Equation (4):

$$M_i = \frac{\Delta A_i}{19} \quad (4)$$

where M_i is the mean annualized area change for class i over the 19-year elapsed interval from 2004 to 2023. These values are descriptive period averages and should not be interpreted as evidence of a constant annual rate. The analysis quantified class-area trajectories but did not identify pixel-to-pixel conversion pathways because a complete transition matrix was unavailable.

2.5 Accuracy Assessment

Classification accuracy was evaluated using producer's accuracy, user's accuracy, overall accuracy, and the Kappa coefficient. Producer's accuracy represents the probability that reference samples of a given class were correctly classified and therefore reflects omission error. User's accuracy represents the probability that pixels assigned to a mapped class actually correspond to that class in the reference data and therefore reflects commission error. Overall accuracy expresses the proportion of correctly classified validation observations, while the Kappa coefficient describes agreement beyond what chance would expect.

The validation dataset was independent of the training samples used for classification. Each validation location was checked individually against Google Earth reference imagery and assigned to the corresponding land-cover class before comparison with the classified map. This procedure was used consistently to derive the class-specific and map-level accuracy statistics reported for each observation year. Classification reliability was interpreted primarily using producer's and user's accuracies because

these measures directly identify class-specific omission and commission errors. Overall accuracy and the Kappa coefficient were retained as supplementary indicators of map-level agreement rather than as the primary basis for evaluating classification reliability (McHugh, 2012). Producer's accuracy was calculated using Equation (5):

$$PA_i = \frac{x_{ii}}{x_{i+}} \times 100 \quad (5)$$

User's accuracy (UA) was calculated using Equation (6):

$$UA_i = \frac{x_{ii}}{x_{+i}} \times 100 \quad (6)$$

Overall accuracy was calculated using Equation (7):

$$OA = \frac{\sum_{i=1}^{r} x_{ii}}{N} \times 100 \quad (7)$$

The Kappa coefficient was calculated using Equation (8):

$$K = \frac{N\sum_{i=1}^{r} x_{ii} - \sum_{i=1}^{r}(x_i + x + i)}{N^2 - \sum_{i=1}^{r}(x_i + x + i)} \quad (8)$$

In these equations, x_{ii} is the number of correctly classified observations for class i, x_{i+} is the row total for class i, x_{+i} is the column total for class i, and N is the total number of validation observations. Formal confidence intervals for class-area estimates were not calculated because the complete confusion-matrix counts and sampling-design information required for design-based uncertainty estimation were unavailable in the analytical archive. Accordingly, the accuracy assessment is interpreted primarily through class-specific producer's and user's accuracies, while overall accuracy and Kappa provide supplementary information on map-level agreement. Spectral similarity among open land, agricultural land, built-up area, and vegetation may produce classification ambiguity, particularly in heterogeneous tropical landscapes. Exposed soil, harvested cropland, dry vegetation, and some built materials may exhibit overlapping spectral responses under specific seasonal or moisture conditions (Dash et al., 2023; Ibrahim, 2023; Melichar et al., 2023).

2.6 Hydrological Interpretation and Evidentiary Boundary

The hydrological significance of land-cover transformation was interpreted using established watershed processes, including changes in rainfall interception, evapotranspiration, soil protection, infiltration opportunity, surface roughness, imperviousness, erosion susceptibility, and flow-path connectivity. Vegetation loss was interpreted as a potential reduction in rainfall interception and soil protection, while built-up expansion was interpreted as a potential increase in imperviousness and rapid drainage connectivity. Agricultural expansion was treated conditionally because its hydrological effects depend on crop cover, tillage practice, soil compaction, slope, and conservation management. Rainfall-station and downstream water-level-recorder locations provide an observational framework for future hydrological analysis. However, the corresponding records were not used to quantify land-cover-attributable changes in discharge. The present study should therefore be understood as a remote-sensing change assessment supported by process-based hydrological interpretation. Quantification of peak flow, runoff volume, lag time, sediment yield, flood depth, or inundation extent would require quality-controlled rainfall and water-level or discharge records, event separation, terrain and soil data, and calibrated hydrological and hydraulic models (Herbei et al., 2024; Liu et al., 2025; Yumol and Santos, 2025). The present study did not estimate river conveyance capacity because the analytical dataset did not include river cross-sectional geometry. Consequently, the mapped land-cover trajectories cannot be used to infer whether individual river reaches have sufficient hydraulic capacity to convey runoff generated under changing watershed conditions.

3. Results and Discussion

3.1 Spatial and Temporal Land-Cover Patterns

The Welang watershed exhibits a pronounced upstream–downstream configuration, with mountainous terrain in the upper basin and a downstream outlet near Pasuruan. Tributaries converge from the western and southern headwaters toward the main river channel. This configuration matters hydrologically because slope, flow-path length, drainage density, and channel proximity affect how quickly rainfall-generated runoff reaches the outlet. Land-cover conversion in upstream and middle watershed zones may therefore influence downstream conditions even when conversion does not occur immediately adjacent to the outlet. The rainfall stations are distributed across upstream, middle, and downstream portions of the watershed and its surrounding area, while the water-level recorder is positioned near the downstream outlet. This monitoring arrangement provides a potentially useful basis for future event-scale analysis, as spatial rainfall variability can be linked to an integrated downstream response. However, a rigorous assessment of flood occurrence and rainfall–runoff response requires synchronized, quality-controlled rainfall and water-level or discharge records; identification of individual flood events; verification of the stage–discharge relationship; and consideration of event rainfall characteristics and antecedent moisture conditions. These hydrometeorological analyses were beyond the scope of the present land-cover assessment; therefore, the current results do not attribute observed flood behavior or changes in downstream response directly to land-cover transformation.

The classified maps indicate substantial spatial transformation between 2004 and 2023 (Figure 2). Vegetation was concentrated mainly in upstream, western, and southern portions of the watershed, whereas agricultural land and built-up areas were more prominent in middle and downstream sectors. Over time, vegetated areas became more fragmented, while agricultural and built-up land expanded across several parts of the basin.

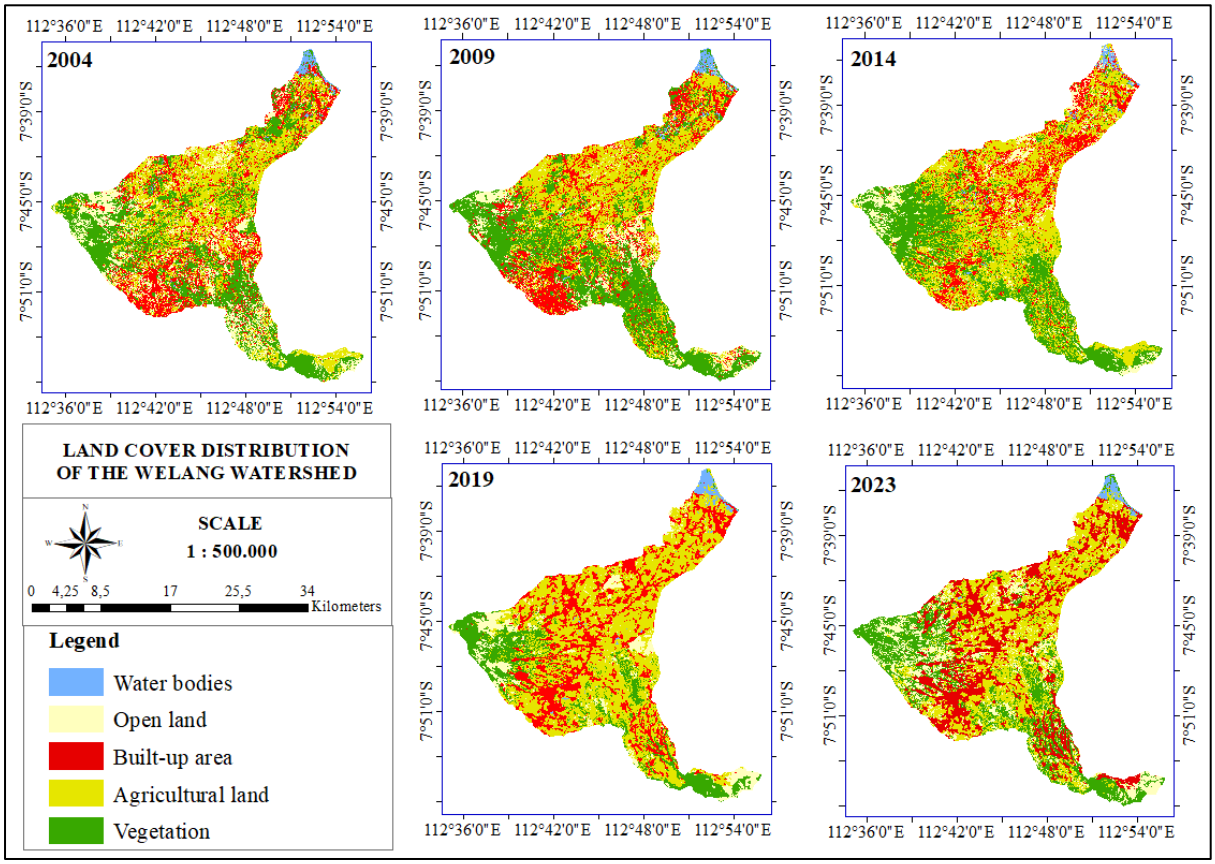


Figure 2. Multi-temporal land-cover distribution in the Welang watershed in 2004, 2009, 2014, 2019, and 2023

The broad spatial trajectories are more reliable than isolated differences between consecutive maps. Built-up and agricultural land expanded persistently, whereas vegetation generally declined. Open land decreased between 2004 and 2019 but increased again in 2023. This non-monotonic pattern may reflect temporary land clearing, agricultural preparation, post-harvest surface exposure, construction activity, or classification confusion among spectrally similar classes. Because exact acquisition dates, crop calendars, and antecedent rainfall conditions were unavailable, the increase in open land in 2023 cannot be attributed confidently to a single process. The spatial arrangement of the land-cover classes is as important as their total area. Built-up or exposed surfaces near drainage channels may contribute runoff more rapidly than comparable surfaces in weakly connected locations. Likewise, vegetation loss on steep slopes may have greater implications for runoff and erosion than vegetation loss on flatter terrain. Previous research has demonstrated that topography, land-cover condition, and drainage connectivity interact in controlling watershed response (Liu et al., 2025; Ongaga et al., 2024). Basin-wide percentages, therefore, provide an important screening indicator but cannot fully capture the spatial distribution of hydrological sensitivity.

3.2 Magnitude and Trajectory of Land-Cover Change

Table 1 summarises the multi-temporal land-cover areas, Table 2 synthesizes the magnitude of change between 2004 and 2023, and Figure 3 illustrates the temporal trajectories. The total watershed area remained constant at 522.90 km², but its land-cover composition changed substantially over the 19 years from 2004 to 2023. The observation intervals were not uniform: the first three intervals were five years, whereas the final interval from 2019 to 2023 was four years. Agricultural land remained the dominant class, increasing from 162.13 km² (31.01%) in 2004 to 190.07 km² (36.35%) in 2023. This represents a net increase of 27.94 km², equivalent to about 17.23% of its 2004 area, and a mean annualized increase of 1.47 km² year^{-1} over the 19 years. Built-up area increased from 104.31 km² (19.95%) in 2004 to 139.18 km² (26.62%) in 2023. The net increase of 34.87 km² represents a relative increase of approximately 33.43% and a mean annualized increase of 1.84 km² year^{-1}. Vegetation declined from 155.72 km² (29.78%) to 110.20 km² (21.07%), representing a loss of 45.52 km² (approximately 29.23% of its 2004 area) and a mean annualized decline of 2.40 km² year^{-1}. Open land decreased by 17.16 km² overall, from 95.31 km² in 2004 to 78.15 km² in 2023, although its trajectory was non-monotonic. Water bodies remained the smallest class and were broadly stable, changing only slightly from 5.43 km² in 2004 to 5.30 km² in 2023. These mapped areas should be interpreted cautiously because river reaches narrower than the 30 m Landsat pixel may be represented by mixed water–land pixels and may therefore be underrepresented or inconsistently classified. Minor temporal fluctuations in the water-body class may consequently reflect a combination of seasonal water conditions, image-acquisition timing, mixed-pixel effects, and classification uncertainty rather than permanent changes in surface-water extent.

Table 1. Land-cover area in the Welang watershed from 2004 to 2023

Classification	2004 km²	2004 %	2009 km²	2009 %	2014 km²	2014 %	2019 km²	2019 %	2023 km²	2023 %
Water bodies	5.4	1.0	6.5	1.2	6.2	1.2	8.3	1.6	5.3	1.0
Open land	95.3	18.2	84.5	16.2	70.2	13.4	57.6	11.0	78.2	14.9
Built-up area	104.3	19.9	112.8	21.6	123.9	23.7	131.8	25.2	139.2	26.6
Agricultural land	162.1	31.0	166.5	31.8	172.4	33.0	188.1	36.0	190.1	36.3
Vegetation	155.7	29.8	152.6	29.2	150.2	28.7	137.1	26.2	110.2	21.1
Total	522.9	100.0	522.9	100.0	522.9	100.0	522.9	100.0	522.9	100.0

Table 2. Land-cover changes in the Welang watershed between 2004 and 2023

Classification	Absolute area change (km²)	Relative change (%)	Percentage-point change	Mean annualized change (km² year^{-1})
Water bodies	−0.13	−2.39	−0.02	−0.01
Open land	−17.16	−18.00	−3.28	−0.90

Classification	Absolute area change (km²)	Relative change (%)	Percentage-point change	Mean annualized change (km² year⁻¹)
Built-up area	+34.87	+33.43	+6.67	+1.84
Agricultural land	+27.94	+17.23	+5.34	+1.47
Vegetation	−45.52	−29.23	−8.71	−2.40

Note: Positive values indicate expansion, whereas negative values indicate contraction between 2004 and 2023.

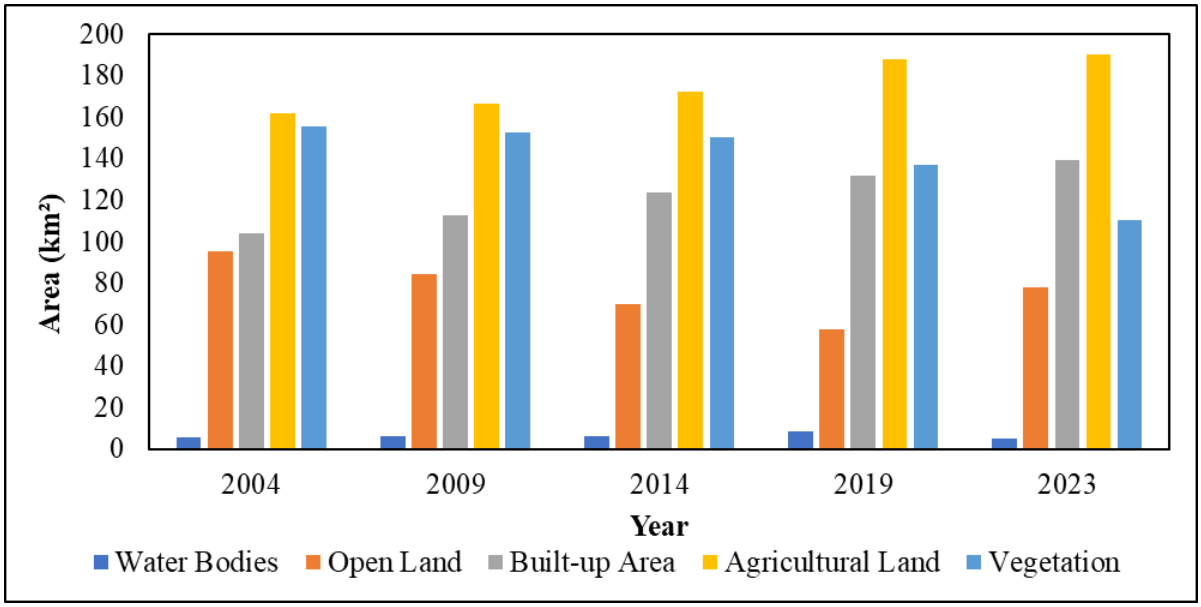


Figure 3. Temporal variation of land-cover classes in the Welang watershed in 2004, 2009, 2014, 2019, and 2023

As summarised in Table 2, built-up area exhibited the largest positive absolute change (+34.87 km²; +6.67 percentage points), whereas vegetation exhibited the largest decline (−45.52 km²; −8.71 percentage points). Agricultural land also expanded substantially (+27.94 km²; +5.34 percentage points), while open land declined (−17.16 km²; −3.28 percentage points) and water bodies remained nearly stable (−0.13 km²; −0.02 percentage points). Consequently, the combined proportion of built-up and agricultural land increased from 50.96% in 2004 to 62.97% in 2023, a 12.01 percentage-point increase. Over the same period, vegetation decreased by 8.71 percentage points. The simultaneous expansion of developed and intensively managed surfaces and the decline in vegetation represent the most important compositional transformation observed in the watershed.

The trajectories were not temporally uniform. Built-up area increased consistently across all observation years, while agricultural expansion accelerated after 2014. Vegetation decline was relatively gradual between 2004 and 2014 but became more pronounced after 2014, particularly between 2019 and 2023. Because the final observation interval (2019–2023) spans four years rather than five, interpret changes during this interval with reference to its shorter duration. The magnitude of the final-interval vegetation decline should nevertheless be interpreted with caution because open land and vegetation exhibited lower class-specific accuracy in 2023 and acquisition-season metadata were unavailable. The current analysis quantifies net class changes but does not identify exact conversion pathways. A pixel-level transition matrix would be required to determine how much vegetation was converted to agricultural land, built-up area, or open land, and whether some locations experienced multiple transitions during the observation period. Such information would strengthen causal interpretation and support more spatially targeted interventions.

3.3 Classification Reliability and Residual Uncertainty

Table 3 presents class-specific classification accuracies. These accuracy statistics were derived from validation samples evaluated independently from the classification training samples using visually interpreted Google Earth reference imagery. Producer's and user's accuracies were used as the primary indicators of classification reliability because they directly quantify class-specific omission and commission errors, respectively. Water bodies exhibited consistently high producer's and user's accuracies across all observation years. Agricultural land also showed high class-specific reliability, with producer's accuracy of 100% in all observation years and user's accuracy ranging from 90% to 100%. In contrast, open land, built-up area, and vegetation showed greater temporal variability in classification performance, consistent with spectral overlap among exposed soil, harvested cropland, sparse vegetation, and developed surfaces. Open land exhibited the lowest producer's accuracy (71% in 2023) and the lowest user's accuracy (75% in 2014), indicating comparatively greater omission and commission errors for this class. Built-up area showed producer's and user's accuracies of 78% in 2019, while vegetation reached 80% producer's accuracy in 2014 and 2023 and 80% user's accuracy in 2004 and 2023. These class-specific accuracy patterns provide a more informative basis for interpreting uncertainty in individual land-cover trajectories than map-level agreement statistics alone.

Table 3. Producer's and user's accuracy of land-cover classification by observation year (%)

Classification		2004	2009	2014	2019	2023
Producer's Accuracy (%)	Water Bodies	100	100	100	100	100
	Open Land	75	83	86	100	71
	Built-up Area	100	88	86	78	100
	Agricultural Land	100	100	100	100	100
	Vegetation	100	100	80	100	80
User's Accuracy (%)	Water Bodies	100	100	100	100	100
	Open Land	100	83	75	100	83
	Built-up Area	88	88	86	78	100
	Agricultural Land	100	100	100	100	90
	Vegetation	80	100	100	100	80

Table 4 reports overall accuracy and Kappa coefficients as supplementary measures of map-level agreement. Overall accuracy ranged from 90.00% to 93.33%, while Kappa coefficients ranged from 0.872 to 0.916. These values indicate consistently high map-level agreement across the five observation years; however, they do not override the class-specific omission and commission errors identified by producer's and user's accuracies.

Table 4. Overall accuracy and Kappa coefficient of the classified land-cover maps

Year	Overall accuracy %	Kappa coefficient
2004	93.33	0.916
2009	93.33	0.915
2014	90.00	0.873
2019	93.33	0.915
2023	90.00	0.872

The combined class-specific and map-level accuracy results support interpretation of the major long-term land-cover trajectories, while also identifying classes and observation years that require greater caution. The net increase of 34.87 km² in built-up area and the net decline of 45.52 km² in vegetation are sufficiently large and directionally persistent that they are unlikely to be explained solely by random classification error. However, high map-level agreement does not eliminate class-specific uncertainty,

particularly for open land, vegetation, and built-up area in observation years with lower producer's or user's accuracies. In particular, the rebound in open land and the substantial reduction in vegetation between 2019 and 2023 may reflect a combination of physical transformation, seasonal surface exposure, and classification ambiguity.

Formal confidence intervals around class-area estimates could not be derived because complete confusion-matrix counts, validation-sample coordinates, and sampling-design information required for design-based uncertainty estimation were unavailable in the analytical archive. Contemporary land-cover studies demonstrate that richer temporal features, terrain variables, independent validation, and statistically representative sampling can improve classification accuracy and enable uncertainty-adjusted area estimation (Dash et al., 2023; Ibrahim, 2023; Melichar et al., 2023). Accordingly, the reported producer's and user's accuracies provide the primary basis for assessing class-specific reliability. In contrast, overall accuracy and Kappa serve as supplementary indicators of map-level agreement rather than substitutes for formal area uncertainty estimates.

3.4 Potential Hydrological and Sediment Implications

Vegetation decline represents the largest net land-cover change detected in the Welang watershed. The loss of 45.52 km² of vegetation indicates a substantial reduction in surfaces that intercept rainfall, protect soil from raindrop impact, maintain root-mediated soil structure, support evapotranspiration, and increase surface roughness. These functions can delay the transfer of rainfall to the drainage network and reduce the susceptibility of exposed soil to detachment and transport. Field evidence from humid tropical forested slopes further indicates that vegetation–soil interactions can modulate rainfall-induced pore-water-pressure dynamics, thereby linking canopy and root-zone processes to slope-scale hydrological response (Hendrayanto et al., 2025). Vegetation loss does not produce a uniform hydrological response because its effects depend on slope, soil depth, antecedent moisture, rainfall intensity, and connectivity to the stream network. Nevertheless, vegetation decline on steep or highly connected terrain may reduce local retention and increase the rate at which excess rainfall reaches tributaries. Remote-sensing and model-based studies have similarly shown that vegetation change can influence runoff generation, evapotranspiration, sediment response, and catchment water balance (Ding et al., 2022; Kang et al., 2024; Sadhwani et al., 2022).

The vegetation remaining in the Welang watershed is concentrated mainly in upstream, western, and southern areas. These locations may be important for watershed regulation because runoff and sediment generated on sloping terrain can be transferred rapidly through the tributary network. The conservation value of vegetation therefore depends not only on its total area but also on its spatial relationship with steep slopes, erosion-prone soils, riparian corridors, and channel-connected flow paths. Research in the Genting watershed demonstrated that conservation priorities can be identified by integrating erosion and sedimentation rates with land conditions and spatial management requirements (Lufira et al., 2022). Applying a similar spatial framework to the Welang watershed would allow ranking vegetation-loss areas by slope, soil erodibility, rainfall erosivity, and channel proximity.

Built-up area exhibited the largest positive absolute change. Developed surfaces can include roofs, roads, compacted ground, settlement infrastructure, and other surfaces that reduce infiltration opportunity. They may also increase hydrological connectivity by routing rainfall through roadside drains, artificial channels, and modified stream networks. Urban and peri-urban watershed studies have shown that increasing imperviousness can be associated with larger runoff volumes, shorter response times, and greater flood sensitivity (Banjara et al., 2024; Ongaga et al., 2024). However, the broad built-up class used in this study should not be equated directly with total or directly connected impervious area. A 30 m pixel classified as built-up may contain mixtures of roofs, roads, yards, vegetation, bare soil, and small drainage features. The hydrological effect of built-up expansion therefore depends on settlement density, surface materials, drainage connectivity, stormwater infrastructure, and proximity to

the channel network. The present maps indicate the expansion of developed land but cannot quantify the corresponding increases in the impervious fraction or peak discharge.

Agricultural land increased by 27.94 km² and remained the dominant class throughout the study period. Agricultural expansion is hydrologically important, but its effect is conditional rather than uniform. Fields with continuous crop cover, terracing, mulching, contour cultivation, and well-maintained soil structure may reduce runoff and erosion. In contrast, bare fields, compacted soils, steep cultivation, downslope tillage, and seasonal clearing may increase rainfall excess, overland flow, soil loss, and sediment transport. Model-based studies have shown that agricultural expansion and land-management scenarios can alter surface runoff, water yield, streamflow components, and sediment production (Anggraheni et al., 2025; Costa et al., 2023; Sadhwani et al., 2022). The increase in open land in 2023 may partly represent agricultural preparation, temporary clearing, harvested fields, or conversion toward built-up surfaces. Because the study did not distinguish crop types, growth stages, or management practices, the hydrological effect of agricultural expansion cannot be inferred solely from its mapped area. Soil and water conservation should therefore be differentiated according to slope, crop cover, soil properties, and stream connectivity. Relevant practices include contour planting, terracing, vegetative strips, mulching, cover crops, riparian buffers, check structures, and controlled drainage. Lufira et al. (2022) emphasized spatial conservation based on erosion and sedimentation conditions, while Haribowo et al. (2019) demonstrated the potential effectiveness of an environmentally compatible sediment-trap model for controlling sediment transported from agricultural land.

3.5 Integrated Interpretation and Evidentiary Boundary

The combined expansion of built-up and agricultural land, accompanied by vegetation loss, indicates a compositional shift toward surface conditions that may more rapidly generate and connect runoff. This result matters not only for net area changes but also for the coherence of the multi-temporal trajectory. Built-up area expanded consistently across the observation years, agricultural land increased overall, and vegetation declined substantially over the long term. Together, these class-specific trajectories indicate a sustained reorganization of watershed surface composition rather than a simple difference between two endpoint maps. The combined proportion of built-up and agricultural land increased from 50.96% in 2004 to 62.97% in 2023, while vegetation declined from 29.78% to 21.07%, providing quantitative evidence of the direction and magnitude of this long-term transformation.

This interpretation is physically plausible because developed surfaces can reduce infiltration opportunities, exposed or compacted agricultural soils can increase excess rainfall, and vegetation loss can reduce interception, surface protection, and flow resistance. However, the hydrological influence of each transition depends on rainfall intensity, antecedent moisture, soil properties, slope, drainage configuration, and channel routing. The basin-scale expression of these land-cover changes is also conditioned by watershed morphometry, because relief, basin shape, drainage density, and stream-network configuration regulate runoff concentration and its subsequent transfer to the watershed outlet (Suharyanto et al., 2020). The present results are consistent with calibrated studies reporting changes in runoff and sediment response following urbanization, agricultural expansion, and vegetation conversion (Banjara et al., 2024; Costa et al., 2023; Ongaga et al., 2024; Sadhwani et al., 2022). Nevertheless, those studies used hydrological models or jointly analyzed imperviousness and runoff, whereas the present study is based on land-cover classification. Accordingly, the mapped trajectories establish the direction and magnitude of long-term landscape transformation and support interpretation of potential runoff and erosion sensitivity. Quantitative changes in discharge, runoff volume, sediment yield, or flood extent require subsequent analysis using quality-controlled hydrometeorological observations and calibrated hydrological or hydraulic models. The mapped land-cover states therefore provide a quantitative baseline for such future assessment.

3.6 Management Priorities and Future Research

The observed land-cover trajectories indicate that watershed management should prioritize hydrologically connected areas rather than rely solely on total class area. Protect remaining vegetation in steep upstream zones, riparian corridors, erosion-prone soils, and areas directly connected to tributaries. Agricultural conservation should be adapted to slope, soil condition, crop cover, and stream proximity through contour cultivation, terracing, mulching, vegetative strips, and riparian buffers. Spatially targeted conservation based on erosion and sedimentation characteristics can improve intervention effectiveness (Lufira et al., 2022), while environmentally compatible sediment traps may complement source-area erosion control at runoff-concentration points (Haribowo et al., 2019). Built-up expansion requires stormwater-sensitive planning, particularly in the middle and downstream watershed. Specific measures may include infiltration wells, permeable pavements, bioretention or vegetated infiltration areas, and detention or retention facilities to reduce rapid surface-runoff connectivity where local soil, slope, groundwater, and drainage conditions are suitable. Areas demonstrated through site-specific assessment to have relatively high infiltration capacity should be protected from unnecessary sealing and incorporated into decentralized rainwater-management systems. Protecting natural drainage corridors and controlling development in riparian and flood-prone zones should complement these measures. Land-cover planning should also integrate water-allocation and economic considerations because changes in agriculture, vegetation, and settlement may influence irrigation demand, sediment-related maintenance, and downstream water availability (Satyagraha et al., 2018).

Future research should develop pixel-level transition matrices and identify conversion hotspots according to slope, soil properties, erosion susceptibility, sub-watershed, and distance to streams. Predictive transition modeling could extend the observed trajectories into alternative future scenarios, as demonstrated using a CA–ANN framework in an Indonesian urban watershed (Lufira et al., 2026). Use the available rainfall stations and downstream water-level recorder to establish quality-controlled rainfall–runoff datasets and a verified stage–discharge relationship. A complementary hydrometeorological assessment should establish a chronology of flood events and analyze event-scale rainfall characteristics using synchronized, quality-controlled observations from the available rainfall stations together with downstream water-level or discharge records. Such analysis should consider rainfall magnitude and temporal distribution, antecedent moisture conditions, and a verified stage–discharge relationship to distinguish rainfall-driven variability from the potential influence of changing land-cover conditions. Future hydraulic assessment should additionally incorporate measured river cross-sectional geometry to evaluate channel conveyance capacity and determine whether changes in runoff-generating conditions may translate into hydraulic constraints along critical river reaches. Where gauge coverage or temporal completeness is insufficient, satellite precipitation products should be locally evaluated and bias-corrected against available station observations; this requirement has been demonstrated specifically for GPM-IMERG precipitation in the Welang watershed (Suhartanto et al., 2025). Calibrated hydrological models could evaluate changes in runoff volume, peak discharge, and lag time under the five mapped land-cover conditions, while hydraulic modeling could translate simulated flows into flood depth and inundation extent (Herbei et al., 2024; Liu et al., 2025; Yumol and Santos, 2025).

4. Conclusions

The Welang watershed underwent substantial land-cover transformation during the 19-year elapsed study period from 2004 to 2023. Built-up area increased by 34.87 km² and agricultural land by 27.94 km², while vegetation declined by 45.52 km². Consequently, the combined proportion of built-up and agricultural land increased from 50.96% to 62.97% of the watershed. Class-specific producer's and user's accuracies indicated generally high classification reliability, although uncertainty was greater for open land, built-up area, and vegetation in some observation years; overall accuracy ranged from 90.00% to 93.33%. The observed transformation therefore represents not only a change in land-cover composition

but also a long-term shift toward more intensively managed and developed surface conditions with potential implications for runoff generation, erosion susceptibility, and watershed management. Across the five observation years, the coordinated trajectories of built-up expansion, agricultural expansion, and vegetation decline demonstrate a coherent long-term reorganization of watershed surface composition rather than an isolated difference between endpoint maps. This trajectory-based evidence is the study's principal empirical contribution and provides a quantitative baseline for subsequent calibrated hydrological assessment and spatial watershed management. Vegetation loss and built-up expansion are consistent with reduced rainfall interception, lower infiltration opportunity, weaker soil protection, and faster runoff connectivity. In contrast, the hydrological effects of agricultural expansion depend on crop cover, slope, soil conditions, and conservation practices. Accordingly, the findings indicate increased potential runoff and erosion sensitivity rather than measured changes in discharge or flood magnitude. The results support protecting hydrologically connected vegetation, targeted agricultural soil and water conservation, sediment-control measures, and stormwater-sensitive planning that incorporates infiltration wells, permeable surfaces, and detention or retention facilities where site conditions allow in expanding built-up areas. Future research should integrate pixel-level land-cover transitions with slope, soil properties, erosion susceptibility, stream connectivity, rainfall observations, and calibrated discharge data. This integration is needed to quantify how land-cover transformation affects runoff volume, peak discharge, sediment yield, and downstream flood extent.

Acknowledgement

The authors sincerely thank the United States Geological Survey (USGS) for providing the Landsat satellite imagery used in this study. The authors also thank the Water Resources Public Works Agency of East Java Province (*Dinas Pekerjaan Umum Sumber Daya Air Provinsi Jawa Timur*) for providing rainfall and downstream water-level data for the Welang watershed. The authors are also grateful to all parties who provided technical support and assistance in completing this research.

Ethics Statement

This study did not involve human participants, animal experiments, or clinical data. Therefore, ethical approval and informed consent were not applicable. The study used satellite imagery, spatial datasets, rainfall observations, and downstream water-level records for environmental analysis.

CRediT Author Statement

Rizki Tri Utami: Idea Development, Formal Analysis, Data Curation, Visualization, Data Verification, Result Verification, Manuscript Draft Preparation. **Ussy Andawayanti:** Research Design, Supervision, Manuscript Review and Revision. **Ery Suhartanto:** Research Design, Investigation, Supervision, Manuscript Review and Revision. **Rahmah Dara Lufira:** Supervision, Result Verification, Manuscript Review and Revision. **Rizki Ramadhani Pratama:** Supervision, Visualization Review, Manuscript Review and Revision.

Data Availability Statement

Landsat imagery is publicly available through the United States Geological Survey. Rainfall and downstream water-level data obtained from the Water Resources Public Works Agency of East Java Province (*Dinas Pekerjaan Umum Sumber Daya Air Provinsi Jawa Timur*) are subject to the agency's data-access conditions. The corresponding author may make the processed land-cover data and available validation summaries available upon reasonable request, subject to institutional and data-ownership permissions.

Declaration of Artificial Intelligence Use

The authors used QuillBot, SciSpace, and Grammarly during manuscript preparation to support language refinement, literature discovery, and clarification of causal interpretations. These tools were not used for data analysis, scientific decision-making, or the generation of results. The authors subsequently reviewed, verified, and revised all content and assume full responsibility for the integrity, accuracy, and final content of the article.

References

Alexopoulos, M.J., Müller-Thomy, H., Nistahl, P., Šraj, M. and Bezak, N. 2023. Validation of precipitation reanalysis products for rainfall-runoff modelling in Slovenia. Hydrology and Earth System Sciences 27, 2559–2581.

Al-Taei, A.I., Alesheikh, A.A. and Darvishi Boloorani, A. 2023. Land use/land cover change analysis using multi-temporal remote sensing data: A case study of Tigris and Euphrates Rivers Basin. Land 12, 1101.

Amini, S., Saber, M., Rabiei-Dastjerdi, H. and Homayouni, S. 2022. Urban land use and land cover change analysis using Random Forest classification of Landsat time series. Remote Sensing 14, 2654.

Anggraheni, E., Hamdany, A.H., Maricar, F., Andika, N., Sisinggih, D., Tanlie, F.S. and Respati, F.A.R. 2025. Hydrological response of land use and climate change impact on sediment rate in Upper Citarum Watershed. Fluids 10, 36.

Banjara, M., Bhusal, A., Ghimire, A.B. and Kalra, A. 2024. Impact of land use and land cover change on hydrological processes in urban watersheds: Analysis and forecasting for flood risk management. Geosciences 14, 40.

Chawanda, C.J., Nkwasa, A., Thiery, W. and van Griensven, A. 2024. Combined impacts of climate and land-use change on future water resources in Africa. Hydrology and Earth System Sciences 28, 117–138.

Costa, R.C.A., Santos, R.M.B., Fernandes, L.F.S., Carvalho de Melo, M., Valera, C.A., Valle Junior, R.F., Silva, M.M.A.P.M., Pacheco, F.A.L. and Pissarra, T.C.T. 2023. Hydrologic response to land use and land cover change scenarios: An example from the Paraopeba River Basin based on the SWAT model. Water 15, 1451.

Dash, P., Sanders, S.L., Parajuli, P. and Ouyang, Y. 2023. Improving the accuracy of land use and land cover classification of Landsat data in an agricultural watershed. Remote Sensing 15, 4020.

Ding, Y., Feng, H. and Zou, B. 2022. Remote sensing-based estimation on hydrological response to land use and cover change. Forests 13, 1749.

Gebrechorkos, S.H., Leyland, J., Dadson, S.J., Cohen, S., Slater, L., Wortmann, M., Ashworth, P.J., Bennett, G.L., Boothroyd, R., Cloke, H., Delorme, P., Griffith, H., Hardy, R., Hawker, L., McLelland, S., Neal, J., Nicholas, A., Tatem, A.J., Vahidi, E., Liu, Y., Sheffield, J., Parsons, D.R. and Darby, S.E. 2024. Global-scale evaluation of precipitation datasets for hydrological modelling. Hydrology and Earth System Sciences 28, 3099–3118.

Gorelick, N., Hancher, M., Dixon, M., Ilyushchenko, S., Thau, D. and Moore, R. 2017. Google Earth Engine: Planetary-scale geospatial analysis for everyone. Remote Sensing of Environment 202, 18–27.

Haribowo, R., Andawayanti, U. and Lufira, R.D. 2019. Effectivity test of an eco-friendly sediment trap model as a strategy to control erosion on agricultural land. Journal of Water and Land Development 42, 76–82.

Hendrayanto, H., Amirul Fata, Y., Askari, M., Erizal, E., Tarigan, S.D. and Suhartanto, E. 2025. The pore water pressure changes on forested slopes in tropical humid climate area. Journal of Ecological Engineering 26, 121–136.

Herbei, M.V., Bădăluță-Minda, C., Popescu, C.A., Horablaga, A., Dragomir, L.O., Popescu, G., Kader, S. and Sestras, P. 2024. Rainfall-runoff modeling based on HEC-HMS model: A case study in an area with increased groundwater discharge potential. Frontiers in Water 6, 1474990.

Ibrahim, S. 2023. Improving land use/cover classification accuracy from Random Forest feature

importance selection based on synergistic use of Sentinel data and digital elevation model in agriculturally dominated landscape. Agriculture 13, 98.

Kang, Y., Zhang, K., Zhang, Y. and Zhao, L. 2024. Hydrological response to vegetation restoration and urban sprawl in typical hydrologic years within a semiarid river basin in China. Frontiers in Environmental Science 12, 1410918.

Liu, H., Yan, H. and Guan, M. 2025. Evaluating the effects of topography and land use change on hydrological signatures: A comparative study of two adjacent watersheds. Hydrology and Earth System Sciences 29, 2109–2132.

Lufira, R.D., Andawayanti, U., Asmaranto, R., Suhartanto, E., Azzahra, A., Utami, R.T. and Rahmawan, I.T. 2026. Hybrid cellular automata-artificial neural network land use change QGIS-MOLUSCE for urban watershed resilience. Journal of Water and Land Development 69, 15–23.

Lufira, R.D., Andawayanti, U., Cahya, E.N. and Dianasari, Q. 2022. Land conservation based on erosion and sedimentation rate (case study of Genting Watershed Ponorogo Regency). Physics and Chemistry of the Earth, Parts A/B/C 126, 103143.

McHugh, M.L. 2012. Interrater reliability: The kappa statistic. Biochemia Medica 22(3), 276–282.

Melichar, M., Didan, K., Barreto-Muñoz, A., Duberstein, J.N., Jiménez Hernández, E., Crimmins, T., Li, H., Traphagen, M., Thomas, K.A. and Nagler, P.L. 2023. Random Forest classification of multitemporal Landsat 8 spectral data and phenology metrics for land cover mapping in the Sonoran and Mojave Deserts. Remote Sensing 15, 1266.

Ongaga, C.O., Makokha, M., Obiero, K., Kipkemoi, I. and Diang'a, J. 2024. Urbanization and hydrological dynamics: A 22-year assessment of impervious surface changes and runoff in an urban watershed. Frontiers in Water 6, 1455763.

Roy, D.P., Kovalskyy, V., Zhang, H.K., Vermote, E.F., Yan, L., Kumar, S.S. and Egorov, A. 2016. Characterization of Landsat-7 to Landsat-8 reflective wavelength and normalized difference vegetation index continuity. Remote Sensing of Environment 185, 57–70.

Sadhwani, K., Eldho, T.I., Jha, M.K. and Karmakar, S. 2022. Effects of dynamic land use/land cover change on flow and sediment yield in a monsoon-dominated tropical watershed. Water 14, 3666.

Satyagraha, B., Limantara, L.M., Bisri, M. and Andawayanti, U. 2018. Model of water economic value optimization based on the land use change. Journal of Water and Land Development 36, 143–152.

Suhartanto, E., Andawayanti, U., Hidayat, M.N., Lufira, R.D. and Utami, R.T. 2025. A comparative evaluation of bias correction techniques for improving GPM-IMERG precipitation data in the Welang Watershed, Indonesia. Engineering, Technology & Applied Science Research 15, 29935–29941.

Suharyanto, A., Suhartanto, E. and Lesmana, S.B. 2020. Watershed morphometric classification analysis using geographic information system. International Journal of GEOMATE 19(74), 114–122.

Sulianto. 2024. Kalibrasi parameter model tangki berbasis metaheuristik untuk transformasi seri data hujan menjadi limpasan periode harian. Jurnal Teknik Hidraulik 15(2), 113–128.

Wahyudi, H., Aziz, K. and Sumirman, E. 2018. ECO drainage implementation for flood handling in DAS Welang Pasuruan District. International Journal of Civil Engineering and Technology 9(8), 1076–1082.

Yumol, P.J.M. and Santos, F.D. 2025. Hydraulic investigation of the impacts of climate and land cover change on flooding of the Pinacanauan de Ilagan River in Isabela, Philippines. Frontiers in Environmental Science 13, 1604757.